OPTIMIZATION DESIGN ANALYSIS OF MOVABLE ROTATING PLATE TYPE GRADING DEVICE FOR POTATO
/
活动转板式马铃薯分级装置优化设计分析

Haohao ZHAO, Weigang DENG*, Zhiqi REN, Chenglong LIU, Dong YAN, Yansong CAI, Zexin ZHAO [1]
College of Mechanical and Electrical Engineering, Inner Mongolia Agricultural University, Hohhot 010018, China
Tel: 0471-6530905; E-mail: wg_deng@126.com
DOI: https://doi.org/10.35633/inmateh-72-28

Keywords: *movable rotating plate, potato, grading, optimization, ANSYS Workbench*

ABSTRACT
The study focused on enhancing a movable rotating plate type grading device for potatoes, prioritizing safety and weight reduction. By optimizing the body frame and movable rotating plate using ANSYS Workbench 2022, a static analysis was conducted to confirm compliance with design requirements for strength and deformation. The optimized frame experienced a remarkable 32.3% weight reduction. Additionally, the direct optimization module of ANSYS Workbench 2022 was employed to lighten the movable rotating plate, resulting in a 22.86% reduction in the total mass of the device. This research serves as an invaluable reference for the structural design and optimization analysis of potato grading devices.

摘 要
本研究针对活动转板式马铃薯分级装置进行了优化设计，注重其安全性和减轻重量。利用 ANSYS Workbench 2022 对机架和活动转板板进行了优化，并进行了静态分析以确认其满足强度和变形要求。通过优化，机架的重量减轻了 32.3%。此外，利用 ANSYS Workbench 2022 的直接优化模块，轻量化了活动转板，使整个装置的总质量较之前状态减少了 22.86%。该研究为马铃薯分级装置的结构设计和优化分析提供了重要的参考。

INTRODUCTION
Potatoes are one of the most important food crops globally. Although China has the largest potato cultivation area in the world, the level of mechanized potato production is relatively low. Therefore, there is an urgent need for research and development in potato mechanization, especially considering the promotion of potato as a staple food strategy *(Kang, H.B. et al., 2022; Liu, P.L. et al., 2021; Ding, Q.L. et al., 2022)*. Potato grading devices play a crucial role in potato harvesting, and researchers in the field have conducted extensive studies on this topic. Currently, there are various types of potato grading devices available, including roller shaft-type, screen-type, and drum-type devices *(Liu, X., 2022)*. These three grading devices often cause damage to the potatoes during the grading process. Moreover, they have limited grading accuracy and require complex adjustments for different grades, which significantly affects the efficiency of potato grading *(Zhou, J.G., 2022; Yu, J.Y., 2022; Lv, J.Q., 2020)*. Therefore, research was conducted and a potato grading device was designed based on the movable rotating plate principle. This grading device utilizes a movable rotary plate with an adjustable gap, resulting in high grading efficiency and the ability to classify potatoes into three different grades. However, the grading device possesses a high safety factor and is relatively heavy, requiring optimization and improvement measures to address these issues.

The traditional optimization approach, which involves making physical modifications, is time-consuming and expensive. In contrast, the virtual simulation optimization design method can significantly reduce the design cycle and save costs to a great extent *(Gu, L.X., 2019)*. There have been numerous reports on virtual simulation optimization both in China and internationally. *Krasyuk A.M. et al*., *(2021)* utilized an optimality criterion based on ANSYS software for the topology-optimized design of axial fan blades, resulting in a significant 60% reduction in blade mass. *Yan, (2022)* performed the lightweight design of the frame of a tensile machine using ANSYS Workbench. As a result, the equivalent force and total deformation of the optimized model were reduced, leading to a weight reduction of 7.11%. *Ma et al., (2012)* optimized the frame of a light truck using ANSYS and the homogenization method.

[1] *Haohao Zhao, Master Candidate; Weigang Deng, Associate Professor; Zhiqi Ren, Master Candidate; Chenglong Liu, Master Candidate; Dong Yan, Master Candidate; Yansong Cai , Master Candidate; Zexin Zhao, Master Candidate*

This approach resulted in an optimized frame topology that met the volume constraint requirements and minimized total flexibility. *Gadwala William Kery et al., (2022),* conducted the optimization of a sports car rim using ANSYS Workbench finite element analysis. The study identified carbon fiber as a viable material for manufacturing the sports car rim. *Jackis Aukah et al., (2020),* optimized a husked corn dryer using ANSYS Workbench and determined that the air velocity at the collector inlet should be increased to 3 m/s, while the air velocity at the biomass heat exchanger outlet should be increased to 2.8 m/s. *Muhammad Aisha et al., (2019),* employed the finite element method in ANSYS Workbench to optimize the topology of a steering knuckle. The optimization process determined the specific mass that needed to be removed to achieve the desired design. Similarly, *Sharma M.P. et al., (2014)* utilized CREO 2.0 in conjunction with ANSYS Workbench to optimize the shape of the automotive steering knuckle.

Jha et al., (2022) utilized CATIA in conjunction with ANSYS Workbench to optimize and enhance the steering knuckle. *Li et al., (2022)* improved and optimized the base structure of the welding robot using ANSYS Workbench. The original model was analyzed and compared to the improved and optimized solution, successfully achieving the desired optimization objectives. *Feng et al., (2022),* utilized ANSYS Workbench to optimize the design of the fan base of the motor. The structural stresses under various operating conditions were simulated and verified. *Li et al., (2023),* employed the response surface optimization of ANSYS Workbench for the lightweight design of an on-board lens in a specific vehicle. The optimization process resulted in a 20.69% reduction in the total mass of the lens. *Li et al., (2017),* optimized the suspension of the potato excavator using ANSYS Workbench and the response surface method. Through the optimization process, the optimal suspension thickness was determined, effectively reducing deformation.

Analysis of existing studies reveals that the virtual simulation optimization design method, known for its cost-saving and high efficiency advantages, has been rarely reported for the optimization design of potato grading devices. Therefore, considering the issues of a high safety factor and heavy mass in the existing movable rotating plate type grading device for potatoes, in this paper, a virtual simulation optimization method based on ANSYS Workbench 2022 is employed to optimize the design of the body frame and movable rotating plate. In line with the optimization requirements of multiple independent variables and multiple objective functions, the MOGA algorithm was utilized for conducting optimization analysis. This led to the identification of an optimal parameter combination that significantly reduced the weight of both the body frame and the movable rotating plate, while ensuring the desired levels of strength and stiffness are met.

MATERIALS AND METHODS

Movable rotating plate type grading device for potato

A movable rotating plate type grading device for potatoes (as shown in Fig. 1) utilizes the gap size of the movable rotating plate to grade potatoes. The grading principle is depicted in the schematic diagram shown in Fig. 2. The movable rotating plate moves cyclically with the conveying chain, with its bottom in contact with the slide rails on both sides. As the tilting angle of the slide rails changes, the gap between adjacent rotating plates gradually widens. Potatoes of different sizes fall into the potato-collecting device through different gaps.

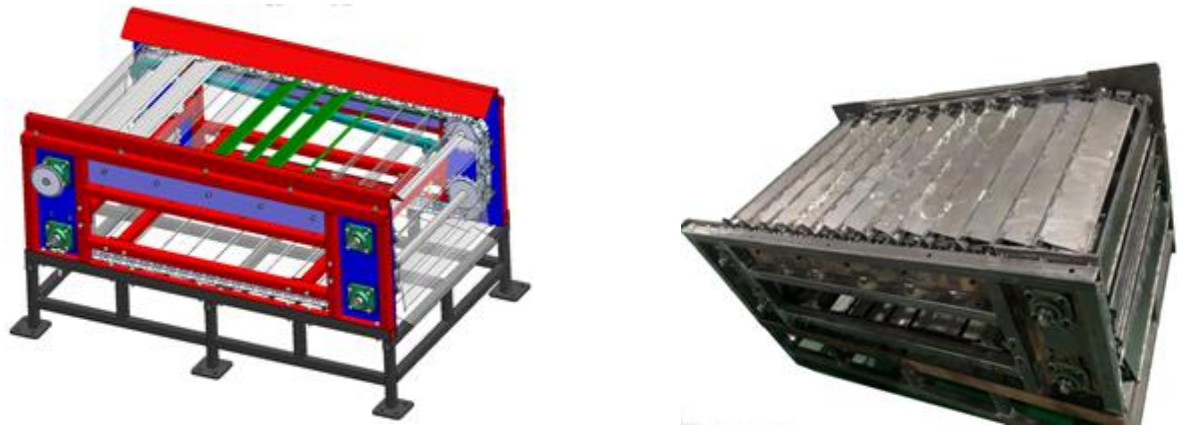

(a) Three-dimensional model diagram (b) Physical diagram

Fig. 1 - Movable rotating plate type grading device for potato

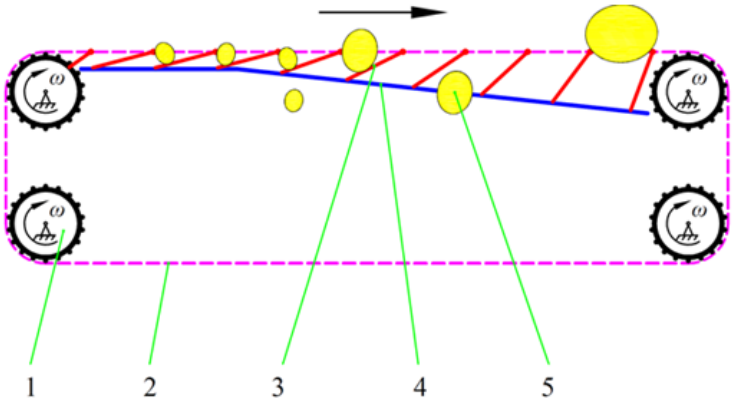

Fig. 2 - Schematic diagram of potato grading principle

1. Sprocket; 2. Chain; 3. Movable rotating plate; 4. Slide; 5. Potato

The body frame (depicted in Fig. 3) consists of the chain fixing part and the base. The chain fixing part primarily serves to secure the chain and the assembly of the movable rotating plate. It is constructed by welding together square steel pipes, with steel plates welded onto the steel pipes to fix the bearing seat. The dimensions of the square steel pipe are 40×40×4 (mm), and the steel plate has a thickness of 8mm. The base is formed by welding together rectangular steel pipes measuring 40×30×3 (mm).

The size of the body frame is 1400×896×780 (mm), and the total mass is 157.82 kg. Due to its high safety factor and large overall mass, the economic performance is below par.

The movable rotating plate (illustrated in Fig. 4) comprises a rotating plate movable shaft, rotating plate, and rotating plate friction shaft, all connected through welding. The rotating plate movable shaft serves as the central component that links the rotating plate to the chain. It is connected to the bracket on the chain section and drives the movement of the rotating plate. The rotating plate friction shaft is in contact with the slide rail and its primary purpose is to prevent direct contact between the rotating plate and the slide rail, thereby minimizing wear and deformation of the rotating plate.

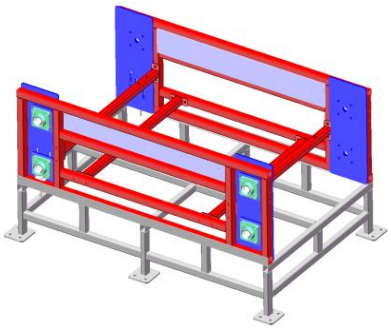

Fig. 3 - Grading device frame

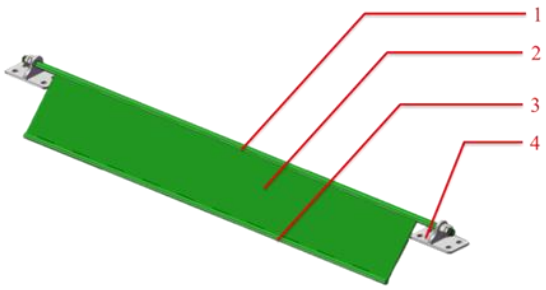

Fig. 4 - Movable rotating plate

1. Rotating plate movable shaft; 2. Rotating plate; 3. Rotating plate friction shaft; 4. Bracket

The dimensions of the existing rotating plate are 640×95×2 (mm) in length, width, and thickness, respectively. The total mass of a single movable rotating plate is 1.7449 kg. With a total of 32 groups of movable rotating plates in the machine, the resulting heavy mass becomes inconvenient for operation.

Static analysis of existing body frame and movable rotating plate

Static analysis of existing body frame

Analysis of load on the body frame

The combined mass of the chain and movable rotating plate assembly (depicted in Fig. 5) amounts to 134.23 kg, while the total mass of the potatoes when the grading device is fully loaded (shown in Fig. 6) is 16.153 kg.

Consequently, the forces exerted on the body frame are as follows.

$$F=(134.23+16.153)\times 9.8=1473.75N \quad (1)$$

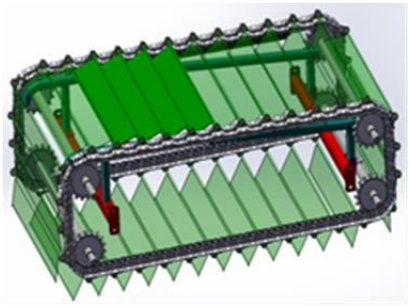

Fig. 5 - Diagram of chain and movable rotating plate assembly

Fig. 6 - A full load of grading device

Pre-processing of the static Analysis of the body frame

According to the design specifications, the body frame is made of Q235 material, and the corresponding material properties are listed in Tab. 1.

Table 1

Material properties

Materials	Density (kg/m^3)	Young's Modulus/Pa	Poisson's Ratio	Yield Strength/Pa	Tangential Modulus/Pa
Q235	7850	2.12×10^{11}	0.288	2.35×10^{8}	6.1×10^{9}

The components of the body frame are joined through a combination of welding and bolting, resulting in a "binding" contact configuration.

When performing an analysis in ANSYS, the size and quality of the mesh divisions at critical locations have a direct impact on the accuracy of the analysis results *(Zhang et al., 2020)*. The denser the mesh divisions, the more accurate the calculation results will be. However, it is important to note that this will also increase the computational volume required for the analysis *(Zhao et al., 2023)*. The frame utilizes an overall tetrahedral meshing method with second-order element ordering, and the mesh cell size is set at 8 mm. However, at the critical force contact position in the bearing seat, a smaller mesh cell size of 3 mm is applied. The completed meshing process yields a total of 1,628,000 nodes and 888,646 cells.

Fixed supports are positioned on the bottom surface of the six foot seats of the body frame, while a combined force of 1473.75 N is applied to the eight bearing surfaces. This results in an equal force of 184.21875 N acting vertically downward on each surface.

The total deformation and equivalent von Mises stress of the body frame were computed, and Fig.7 illustrates the visual representation of the deformation and stress distribution.

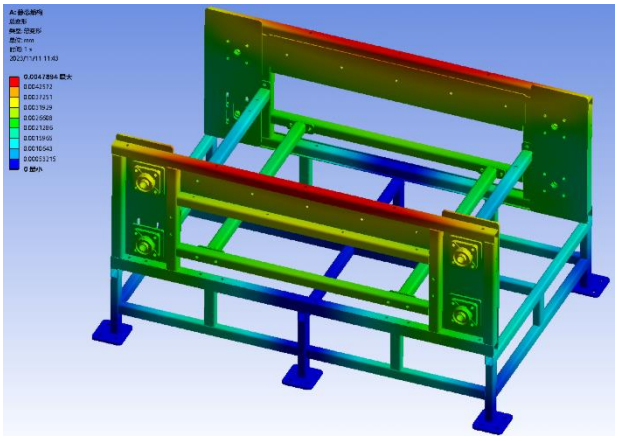

(a) Total Deformation

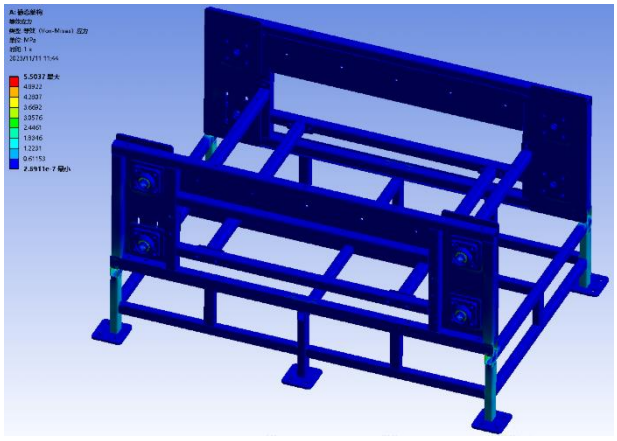

(b) Equivalent von Mises Stress

Fig. 7 - Analysis diagram of the rack before optimization

The cloud diagram of total deformation reveals that the upper steel tube of the body frame experiences more significant deformation. Overall, the deformation gradually decreases from top to bottom, with a maximum deformation of 0.0047894 mm. On the other hand, the cloud diagram of equivalent stress demonstrates that stress is primarily concentrated at the eight bearing positions and the four vertical beams of the base. The maximum stress value recorded is 5.5037 MPa.

In the realm of static analysis in ANSYS, the convergence of forces and displacements serves as pivotal metrics for assessing the convergence and stability of the analysis. They enable the determination of whether the model converged to a stable solution, pinpointing potential issues or errors. The efficacy of force convergence can be evaluated through convergence criteria or residual values, typically requiring force residual values to approach zero, indicative of a reasonable force distribution. A small or gradually stabilizing displacement residual value can suggest that the model is gradually reaching equilibrium. The force convergence and displacement convergence charts are depicted in Fig. 8.

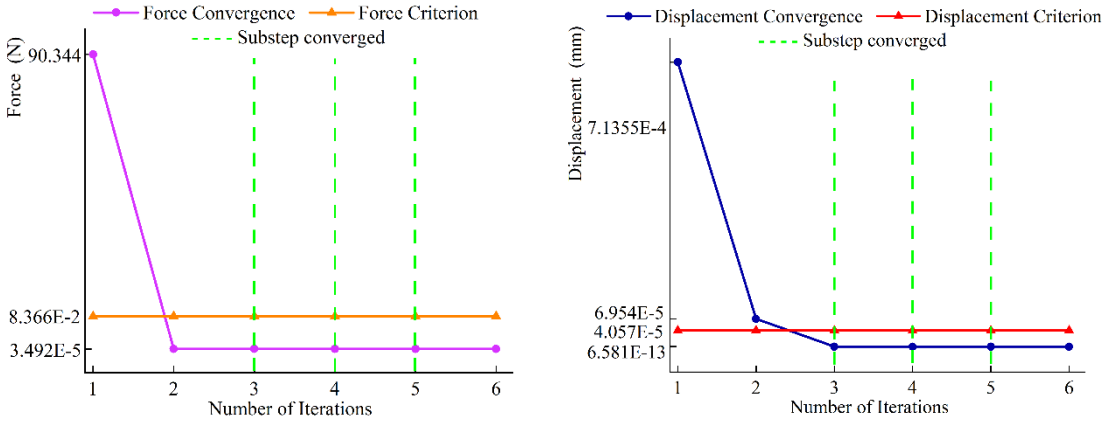

(a) Force convergence (b) Displacement convergence

Fig. 8 - Convergence plot of residual values for the body frame

Based on the analysis results above, it is evident that the current vehicle body frame meets the strength requirements, with a relatively high safety factor, the minimum safety factor being 15, and it possesses sufficient redundancy, as shown in Fig 9. Therefore, there is significant potential for lightweight optimization of the vehicle body frame, providing ample room for improvement.

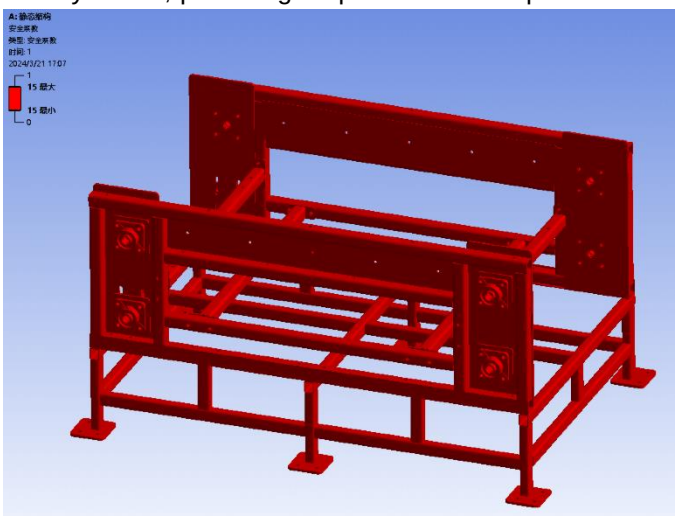

Fig. 9 - Safety factor diagram

Static Analysis of existing movable rotating plate

Calculation of the Load on the movable rotating plate

During the movement of the movable rotating plate, the angle between the plate and the horizontal plane continuously changes from 0 to 90 degrees. When the plate is parallel to the horizontal plane, the maximum load is applied. In order to achieve this maximum load, the entire surface of the rotating plate is covered with potatoes, as depicted in Fig. 10. The total mass of the potatoes is 2.63 kg, equivalent to a force of 25.8 N.

Fig. 10 - Single movable rotating plate covered with potatoes

Statics analysis pre-processing of movable rotating plate

In accordance with the design requirements, the movable rotating plate is made of Q235 material, and its material-related parameters are identical to those of the body frame.

The movable shaft, friction shaft, and rotating plate are welded together, establishing a "fixed" connection between them. The mesh division method employed is "automatic," with a mesh cell size set at 2 mm. This mesh division process generates a total of 426,133 nodes and 250,562 cells.

During the static analysis, fixed constraints are applied to the connection between the rotating plate and the chain, as well as at the contact position with the slide rail. The movable rotating plate is subjected to a downward force of 25.8 N, perpendicular to its surface.

The solution option involved analyzing the total deformation and equivalent von Mises stress. The resulting cloud diagrams illustrating the total deformation and equivalent von Mises stress are presented in Fig. 11. The graphs depicting the convergence of action transfer and displacement transfer are shown in Fig. 12.

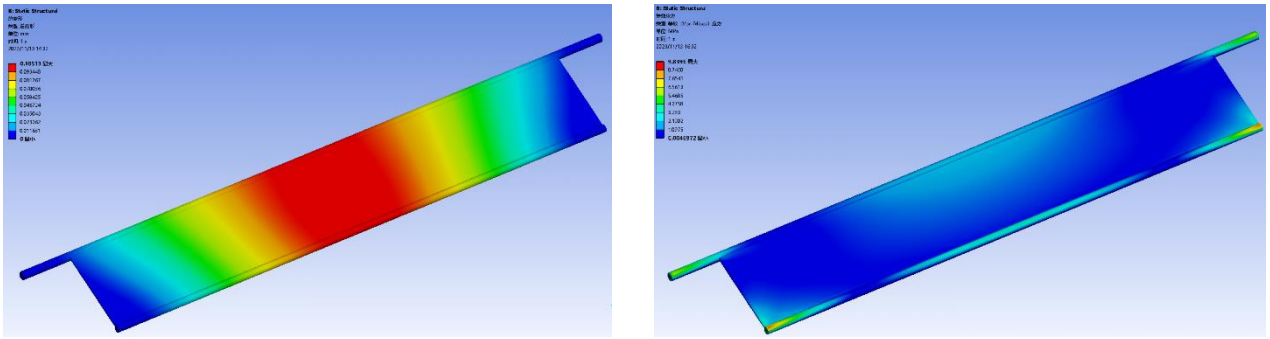

(a) Total Deformation (b) Equivalent von Mises Stress

Fig. 11 - Analysis clouds of the rotating plate before optimization

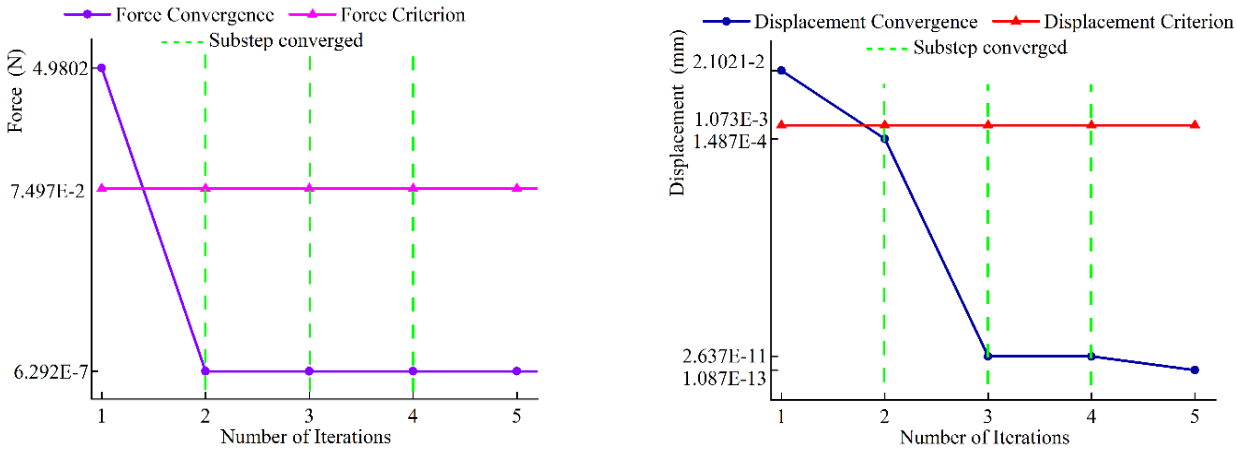

(a) Force convergence (b) Displacement convergence

Fig. 12 - Convergence plot of residual values for the movable rotating plate

The simulation results revealed that the total deformation primarily occurred in the middle section of the rotating shaft, rotating plate, and friction shaft. The overall deformation exhibited a gradual increase from the two ends of the movable rotating plate towards the middle section, reaching a maximum deformation of 0.10513 mm at the central part.

The analysis of the equivalent von Mises stress diagram revealed that the stress concentration was primarily observed at the two ends of the rotating shaft and the friction shaft. This can be attributed to the connection between the bracket and the movable rotating plate shaft at the two ends, causing stress concentration during movement. Additionally, stress concentration was observed at the friction shaft due to contact with the sliding rail. The maximum stress recorded was 9.8396 MPa, which is lower than the material yield strength of 235 MPa.

Based on the aforementioned analysis results, it is evident that the movable rotating plate meets the strength requirements. Therefore, the design can be further optimized by focusing on dimensional parameters.

Optimized design of body frame and movable rotating plate

Body frame optimization design

The wall thickness of the square steel pipe, which forms the body frame, is a critical factor that impacts the structural integrity. Therefore, the wall thickness is reduced from 4 mm to 2 mm. Additionally, the body frame consists of six side plates, each with a thickness of 8 mm, primarily used for fixing the bearing seat and chain brace. Taking into account the high safety factor, the thickness of the side plates is increased to 5 mm. Moreover, the base, being a crucial component that supports the entire machine, undergoes structural improvements as part of the optimization process. The optimized body frame is depicted in Fig. 13, with a total mass of 106.84 kg.

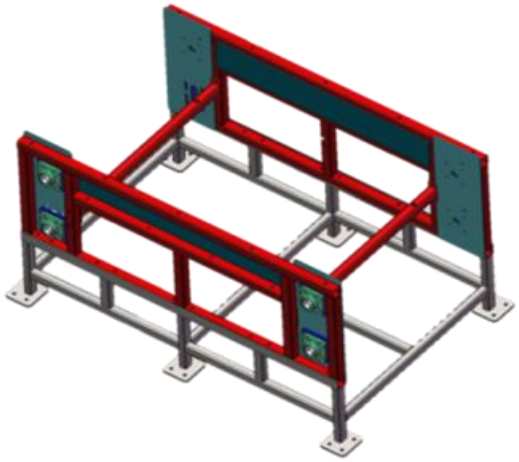

Fig. 13 - Optimized body frame

Optimized design of the movable rotating plate

Rotating plate friction shaft improvement

The current friction shaft for the rotating plate has a diameter of Φ9 mm and a length of 640 mm. Considering its contact position with the slide rail only at the two ends, the friction shaft can be divided into two sections, each measuring 50 mm in length. The schematic diagram of the enhanced friction shaft is depicted in Fig. 14.

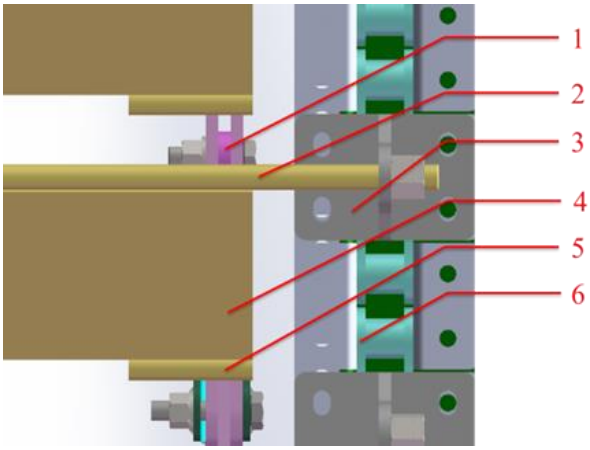

Fig. 14 - Schematic diagram of the improved friction shaft of the rotating plate

1. Slide rail; 2. Rotating plate movable shaft; 3. Bracket; 4. Rotating plate; 5. Rotating plate friction shaft; 6. Chain

Size optimization of rotating plate

For the purpose of optimizing and simplifying the model, the rotating plate friction shaft for the rotary plate was temporarily excluded from the current modelling. Instead, an improved model of the movable rotating plate was created in SolidWorks. The length, width, and thickness of the rotating plate were

defined as the design variables, taking into account the configuration requirements of the Workbench optimization module *(Zhang, 2017; Ren, 2022)*, as shown in Tab. 2.

Table 2

Comparison of relevant parameters before and after frame optimization

Design variable name	Size / mm	Meaning of variables
DS_D1@ thin-stretch1	640	the length of the rotating plate
DS_D2@ sketch2	95	the width of the rotating plate
DS_D3@thin-stretch1	2	the thickness of the rotating plate

The improved model can be seamlessly imported into Workbench using the inter-face between SolidWorks and Workbench, enabling static structural analysis. As per the design requirements, Q235 was chosen as the material for the movable rotating plate. The design variables were selected within the Design Modeler, rendering the model prepared for static structural analysis.

The rotating shaft and rotating plate were welded together, resulting in a "bonded" contact. The mesh division method employed was "Automatic." A mesh cell size of 2 mm was selected, generating a total of 211,015 nodes and 80,593 cells through the grid division process. The grid quality of the movable rotating plate met the requirements, as confirmed by the grid evaluation statistics provided by Workbench.

The fixed restraints and applied loads on the movable rotating plate remained the same as described in the previous section.

The total deformation and equivalent von Mises stress of the model were analyzed in the solution option, resulting in the generation of cloud diagrams illustrating the total deformation and equivalent von Mises stress. These diagrams are presented in Fig. 15.

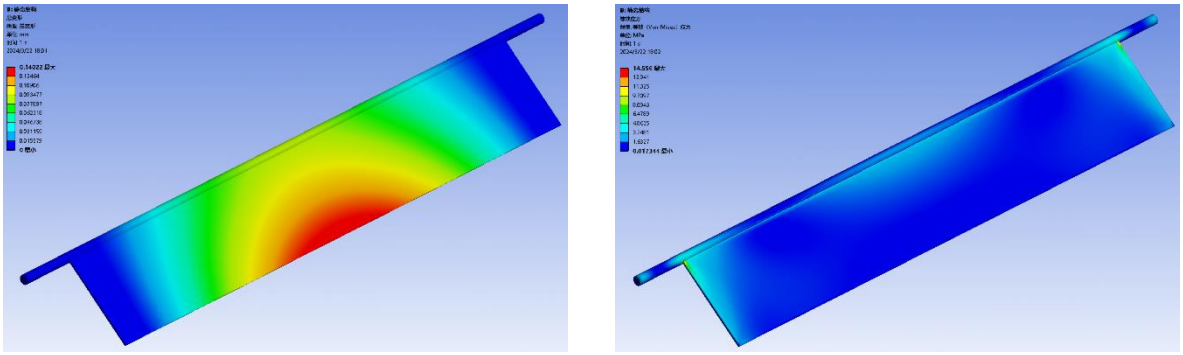

(a) Total Deformation (b) Equivalent von Mises Stress

Fig. 15 - Analysis clouds of the movable rotating plate before optimization

The cloud diagram depicting the total deformation, derived from the simulation results, revealed that the primary deformation occurred in the middle section of the rotating plate and the central part of the rotating shaft. The maximum deformation recorded was 0.14022 mm. On the other hand, the equivalent von Mises stress analysis indicated a maximum stress value of 14.556 MPa.

Structural optimization typically involves adjusting the design variables to enhance the performance of the structure without compromising its functionality, while ensuring compliance with any imposed constraints *(Cha, 2015)*. By modifying the dimensional parameters of the rotating plate, the objective is to minimize its mass while ensuring that both deformation and stresses remain within acceptable limits and maintain a satisfactory safety factor.

This optimization design employs the direct optimization module within Work-bench to seek the optimal combination of dimensional parameters for the rotating plate. As such, the length P_1, width P_2, and thickness P_3 of the rotating plate are treated as design variables. The selection of size ranges is primarily determined by usage and manufacturing requirements. The optimization objectives include maximizing the maximum deformation P_4, maximizing the maximum equivalent force P_5, and minimizing the mass P_6 of the rotating plate. The stress is considered as a safety factor with a value of 1.5, resulting in an allowable stress of 156 MPa. Hence, the minimum stress must not exceed 156 MPa. The optimization design problem can be mathematically formulated as follows:

$$\begin{cases} \min \begin{cases} p_4 = f_1(p_1, p_2, p_3) \\ p_5 = f_2(p_1, p_2, p_3) \leq 156MPa \\ p_6 = f_3(p_1, p_2, p_3) \end{cases} \\ s.t. \begin{cases} p_1 \in (610, 616, 620, 640) \\ p_2 \in (95, 98, 100) \\ p_3 \in (1, 1.2, 1.5, 1.8, 2) \end{cases} \end{cases} \quad (2)$$

Building a direct optimization model

To establish a direct optimization model, the optimization algorithm must first be defined. In the field of multivariate and multi-objective optimization algorithms, two commonly used methods are the Screening algorithm and the MOGA algorithm. These algorithms differ in their objectives and application domains. The Screening algorithm is primarily used for feature selection and dimensionality reduction, aiming to improve model interpretability and computational efficiency. On the other hand, the MOGA algorithm is specifically designed to tackle multi-objective optimization problems by identifying a set of non-dominated solutions, providing decision-makers with a range of choices across multiple objectives. Considering the optimization requirements of multiple independent variables and multiple objective functions in this article, the MOGA algorithm was chosen for the optimization analysis. The MOGA algorithm excels in handling multiple objectives and constraints, and it requires continuous input parameters. It is particularly effective in calculating global maxima or minima, enabling the identification of the global optimum while mitigating the limitations associated with local optima *(Zuo, 2023; Chen, 2015)* In the configuration of the MOGA algorithm, the initial sample capacity was set to 100, generating 50 samples per iteration. The maximum number of iterations was defined as 20, and the restriction of a maximum of 3 candidates was applied.

The objectives and constraints for the rotating plate length P_1, width P_2, and thickness P_3 were established based on the aforementioned mathematical model. Following the parameter settings, the optimization scheme was updated, and subsequently, the solution was initiated.

The total deformation, equivalent von Mises stress, and mass of the model were obtained for various cases of the rotating plate length, width, and thickness by analyzing the 60 sets of design solutions. The results are presented in Tab. 3.

Table 3

Raw optimization data

Serial number	P_1 / mm	P_2 / mm	P_3 / mm	P_4 / mm	P_5 / MPa	P_6 / kg
1	610	95	1	0.335376	31.37097	0.924593
2	616	95	1	0.33314	31.54316	0.929073
3	620	95	1	0.338713	31.4189	0.93206
4	640	95	1	0.343188	33.55511	0.946994
5	610	98	1	0.353951	31.02046	0.938977
6	616	98	1	0.351401	31.18514	0.943598
7	620	98	1	0.357154	31.05804	0.946679
8	640	98	1	0.36119	33.17132	0.962085
9	610	100	1	0.366924	30.81309	0.948566
10	616	100	1	0.364175	30.97273	0.953282
11	620	100	1	0.370046	30.84402	0.956426
12	640	100	1	0.373807	32.94609	0.972146
13	610	95	1.2	0.247201	26.80225	1.01569
14	616	95	1.2	0.246619	26.99724	1.021066
15	620	95	1.2	0.250821	26.8091	1.024651

Serial number	P_1 / mm	P_2 / mm	P_3 / mm	P_4 / mm	P_5 / MPa	P_6 / kg
16	640	95	1.2	0.25723	28.43592	1.042571
17	610	98	1.2	0.258042	26.48829	1.032951
18	616	98	1.2	0.257254	26.67827	1.038497
19	620	98	1.2	0.261565	26.4883	1.042194
20	640	98	1.2	0.267701	28.09787	1.060681
21	610	100	1.2	0.265646	26.29697	1.044458
22	616	100	1.2	0.26473	26.48342	1.050117
23	620	100	1.2	0.269111	26.29202	1.05389
24	640	100	1.2	0.275079	27.8929	1.072754
25	610	95	1.5	0.178684	21.59502	1.152336
26	616	95	1.5	0.179551	21.69055	1.159057
27	620	95	1.5	0.1823	21.58057	1.163537
28	640	95	1.5	0.189913	22.48546	1.185938
29	610	98	1.5	0.184138	21.33209	1.173912
30	616	98	1.5	0.184898	21.4249	1.180844
31	620	98	1.5	0.187684	21.31408	1.185466
32	640	98	1.5	0.195152	22.20793	1.208575
33	610	100	1.5	0.188006	21.16695	1.188296
34	616	100	1.5	0.1887	21.25752	1.19537
35	620	100	1.5	0.19151	21.14581	1.200086
36	640	100	1.5	0.198891	22.03336	1.223666
37	610	95	1.8	0.140836	17.79926	1.288982
38	616	95	1.8	0.142329	17.86102	1.297047
39	620	95	1.8	0.14429	17.78071	1.302423
40	640	95	1.8	0.15203	18.18255	1.329304
41	610	98	1.8	0.143799	17.57471	1.314873
42	616	98	1.8	0.145232	17.63877	1.323192
43	620	98	1.8	0.147198	17.55431	1.328738
44	640	98	1.8	0.154848	17.94952	1.356468
45	610	100	1.8	0.145937	17.43167	1.332134
46	616	100	1.8	0.147335	17.49638	1.340623
47	620	100	1.8	0.149304	17.40931	1.346282
48	640	100	1.8	0.156902	17.80011	1.374578
49	610	95	2	0.129303	14.27097	1.38008
50	616	95	2	0.131227	14.31895	1.38904
51	620	95	2	0.132632	14.2965	1.395014
52	640	95	2	0.140215	14.55594	1.424882
53	610	98	2	0.131863	14.06587	1.408847

Serial number	P_1 / mm	P_2 / mm	P_3 / mm	P_4 / mm	P_5 / MPa	P_6 / kg
54	616	98	2	0.133774	14.11403	1.418091
55	620	98	2	0.135171	14.08991	1.424253
56	640	98	2	0.142727	14.34426	1.455064
57	610	100	2	0.133604	13.93621	1.428026
58	616	100	2	0.135506	13.9844	1.437458
59	620	100	2	0.1369	13.95889	1.443746
60	640	100	2	0.14444	14.20926	1.475186

RESULTS

Static analysis of optimized body frame

The optimized body frame underwent a static structural analysis using the same mesh division, fixed supports, and load constraints as the original body frame. The analysis yielded results for total deformation and equivalent von Mises stress, which are illustrated in Fig. 16.

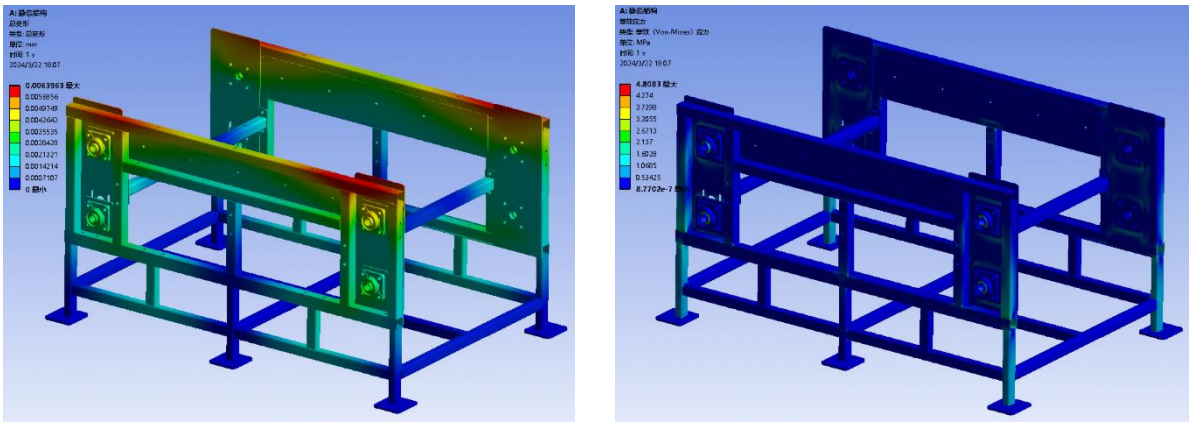

(a) Total Deformation (b) Equivalent von Mises Stress

Fig. 16 - Clouds of optimized body frame analysis results

The final optimized body frame exhibits a maximum total deformation of 0.0063963 mm and a maximum equivalent von Mises stress of 4.8083 MPa. The deformation primarily occurs in the middle section of the steel tube above the frame, but the overall deformation is minimal. Stress concentration is observed at the bearing positions and the vertical beams of the frame base, but the stress levels remain significantly lower than the yield stress.

In conclusion, the optimized body frame successfully meets the strength requirements while significantly reducing the total mass of the machine. A comparison of the relevant parameters before and after the body frame optimization is presented in Tab. 4, demonstrating a remarkable 32.3% reduction in total mass compared to the pre-optimized frame.

Table 4

Comparison of relevant parameters before and after frame optimization

Projects	Steel pipe wall thickness/mm	Side plate thickness/mm	The total mass of frame/kg
Before optimization	4	8	157.82
After optimization	2	5	106.84

Analysis of optimized results from movable rotating plate

The optimization process reached convergence after 1 iteration without any failure points, resulting in three sets of optimal solutions. These solutions are presented in Tab. 5.

Table 5

Optimized design points

Candidate points	P_1 / mm	P_2 / mm	P_3 / mm	P_4 / mm	P_5 / MPa	P_6 / kg
1	610	95	1.2	0.2472	26.802	1.0157
2	616	95	1.2	0.24662	26.997	1.0211
3	620	95	1.2	0.25082	26.809	1.0247

Candidate point 1 was chosen as the ultimate optimization solution. By comparing the design variables and target variables before and after optimization, it is evident that the mass has been reduced by 28.7%. However, there is a slight increase of 0.1 mm in deformation and a 12 MPa increase in stress. Nevertheless, these values remain within the allowable limits, satisfying the strength requirements for the movable rotating plate. The reliability and safety aspects are in accordance with the specified requirements. A comparison of the parameters before and after the optimization of the rotating plate is presented in Tab. 6.

Table 6

Comparison of the parameters before and after the optimization of the rotating plate

Projects	P_1 / mm	P_2 / mm	P_3 / mm	P_4 / mm	P_5 / MPa	P_6 / kg
Before optimization	640	95	2	0.140215	14.55594	1.424882
After optimization	610	95	1.2	0.2472	26.802	1.0157

As mentioned in the previous section, the ANSYS Workbench was utilized for the optimized design of the movable rotating plate. In this design process, the rotating plate friction shaft was not explicitly modelled or optimized. However, after the optimization of the rotating plate structure, the rotating plate friction shaft was included for finite element analysis. By considering the combined effects of the optimized rotating plate and the friction shaft, the final optimized results for the movable rotating plate were obtained. These results are illustrated in Fig. 17.

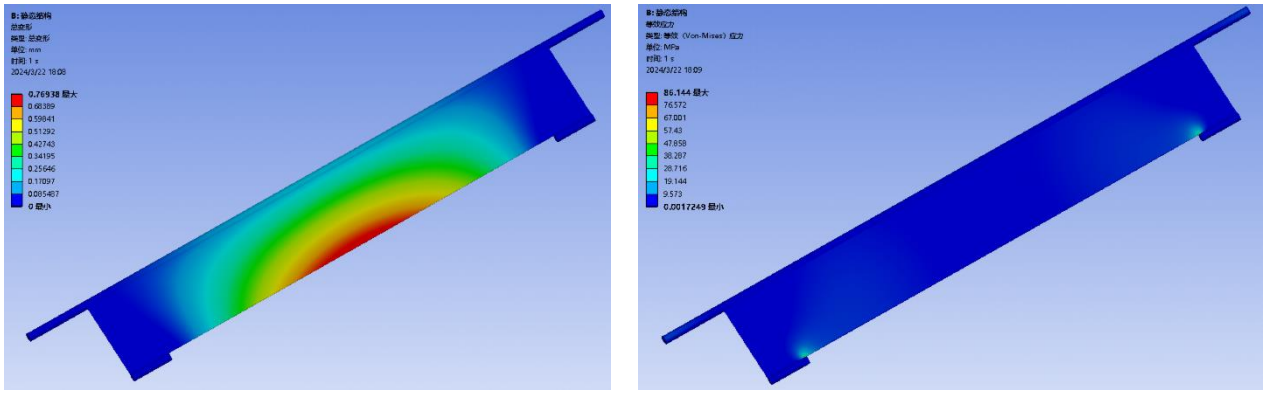

(a) Total Deformation (b) Equivalent von Mises Stress

Fig. 17 - Analysis clouds of the movable rotating plate after optimization

Based on the results of static analysis, the final optimized movable rotating plate demonstrated a maximum deformation of 0.76938 mm, a maximum stress value of 86.144 MPa, and a minimum safety factor of 2.9718. Although the most significant deformation still occurs in the middle section of the rotating plate, it still satisfies the safety and strength requirements. The stress concentration primarily occurs in the movable shaft and friction shafts of the rotating plate. Taking real-world considerations into account, it is necessary to bolt the movable shaft of the rotating plate, and the friction shaft of the rotating plate experiences friction with the slide rail. Nevertheless, the maximum stress remains below the allowable stress of the material.

CONCLUSIONS

The comparison of static structural analysis between the frame and movable rotating plate before and after optimization is presented in Tab. 7.

Table 7

Comparison of the parameters before and after the optimization of the rotating plate

Optimization Project		Mass / kg	Total deformation / mm	Equivalent Stress / MPa
Body frame	Before optimization	157.82	0.0047894	5.5037
	After optimization	106.84	0.0063963	4.8083
Movable rotating plate	Before optimization	1.7449	0.10513	9.8396
	After optimization	1.0657	0.76938	86.144

The original mass of the movable rotating plate was 1.7449 kg, which was reduced to 1.0657 kilograms after optimization, reduction of 38.9% being achieved through the implementation of a lightweight design. The maximum total deformation post-optimization was 0.76938 mm, staying within the acceptable deformation range. The maximum equivalent stress in the optimized movable rotating plate is 86.144 MPa, remaining below the material's yield limit and meeting the strength criteria.

Before the optimization, the mass of the classifier was 320 kg. However, after optimizing the body frame and the movable rotating plate, the mass of the classifier reduced to 246.8456kg. This represents a significant decrease of 22.86% compared to the overall machine mass.

This article utilized the direct optimization module available in ANSYS Workbench to establish a finite element model of the movable rotating plate. Through finite element calculation, simulation, and verification, the optimal combination of dimensional parameters was derived. However, further theoretical and practical validation is necessary to assess the accuracy, reliability, and applicability of the optimization method proposed in this article. The methodology presented in this study offers valuable theoretical guidance for engineering design and structural optimization, effectively mitigating inaccuracies resulting from practical design and saving design time.

ACKNOWLEDGEMENT

This research was funded by the Natural Science Foundation of Inner Mongolia Autonomous Region of China (2022MS05027), Program for improving the Scientific Research Ability of Youth Teachers of Inner Mongolia Agricultural University (BR220127), Scientific Research Start-up Foundation for importing the high level/excellent doctoral talents of Inner Mongolia Agricultural University (NDYB2021-12) and Science and Technology Plan Project of Hohhot (2023-Nong-11).

REFERENCES

[1] Cha, S.; Shang, X. J.; Gang, X. Y. (2015). *Engineering structure optimization design methods and applications (工程结构优化设计方法与应用)*, 1st ed.; China Railway Press: Beijing, China; pp. 1-15.

[2] Chen, X. L.; Liu, Y. J. (2015). *Finite Element Modeling and Simulation with ANSYS Workbench*, 1st ed.; Taylor & Francis Group: Boca Raton, London, New York; pp. 331-356.

[3] Ding, Q.L.; Guo, F.Y. (2022). Key Technologies and Development Trend of Potato Mechanized Harvest (马铃薯机械化收获关键技术及发展趋势), *Agricultural Mechanization Using ＆ Maintenance*, 11, 44–46.

[4] Feng, Y.; Miao, J.; Zheng, L. B.; Wang, X. R. (2022). Optimal Design of Multi-Objective Parameters for Interference Fit of Motor Fan Pedestal based on ANSYS. *Journal of Physics: Conference* Series. 2202, 012044.

[5] Gu, L.X.; Wang, C.G.; Hu. (2019). *Finite Element Analysis and Virtual Simulation of Potato Motion on Oscillating Separation Sieve (马铃薯在摆动分离筛上运动的有限元分析与虚拟仿真研究)*. *The Second Sino-German Symposium on Electromechanical Integration Vocational Education and the Third National Symposium on Electromechanical Integration Professional Teaching Experience Exchange*. pp.48-51, Shandong / China.

[6] Gadwala William Kery; Babu G Raghu. (2022). Modeling and analysis of car wheel rim for weight optimization to use additive manufacturing process. *Materials Today: Proceedings*. 62, 336-345.

[7] Jackis Aukah; Mutuku Muvengei; Hiram Ndiritu; Calvin Onyango. (2020). Optimization of the Performance of Hybrid Solar Biomass Dryer for Drying Maize Using ANSYS Workbench. *Journal of Energy Research and Reviews*. 4. 50-69.

[8] Jha, A.R.; Jaiswal, R.; Karki, A.; Basnet, A.; Jaiswal, S.; Jaiswal. P.; Rajgadia, D. (2016). Design and Finite Element Analysis of Knuckle Joint Using CATIA and ANSYS Workbench. *International Journal of Research in Mechanical Engineering*. 4, 01-05.

[9] Kang, H.B.; Liu, M.; Wang, L.; Wei, M.Y.; Liu, J.C.; Zhou, J.D.; Zhang, S.Q. (2022). Simulation Analysis of Separating and Conveying Device of Potato Harvester Based on EDEM (基于 EDEM 的马铃薯收获机分离输送装置仿真分析). *Journal of Agricultural Mechanization Research*. 44, 1-8.

[10] Krasyuk A. M.; Russky E. Yu. (2021). Optimizing design of blades for high-speed axial fans. *Journal of Mining Science*. 56, 1024–1031.

[11] Liu, P.L.; Zhou, Y.; Zhang, W.J. (2021). Study on production efficiency and its influencing factor of potato production areas in China under the background of main grain production (主粮化背景下中国马铃薯主产区生产效率及其影响因素研究). *Journal of Agricultural Science Yanbian University*. 43, 93–100.

[12] Liu, X. (2022). *Design and Experimental Research on Potato Conveying and Grading Device (马铃薯输送分级装置设计与试验研究)*. Northwest A&F University, Xianyang, Shaanxi, China, May.

[13] Lv, J.Q. (Northeast Agricultural University, Harbin, Heilongjiang, China); Wen, X.Y. (Northeast Agricultural University, Harbin, Heilongjiang, China); Yang, X.H (Northeast Agricultural University, Harbin, Heilongjiang, China). (2020). *Research Status and Prospect of Potato Grader Grading Adjustment Device (马铃薯分级机分级调节装置的研究现状及展望)*. 423-438.

[14] Li, X.J.; Liang, J. (2022). Optimization design and finite element analysis of welding robot base based on ANSYS Workbench. *Journal of Physics: Conference Series*. 2383, 012073.

[15] Li, C. C.; Li, S. Li, M. Z.; Mao, K. (2023). Structural optimization design of vehicle mounted lens for special vehicles (特种车辆的车载镜头轻量化设计). *Agricultural Equipment & Vehicle Engineering*. 61, 144-149.

[16] Li, X.; Wang, C. G.; Deng, W. G.; Xie, S. S.; Wang, X. R. (2017). Static analysis and optimization design of the suspension frame of potato digger (马铃薯挖掘机悬挂架的静力学分析与优化设计). *Chinese Journal of Construction Machinery*. 2017, 15, 42-46.

[17] Ma, C.B.; Wu, Y.H. (2012). Optimize Design of a Light Truck Frame. *Advanced Materials Research*. 590, 346-351.

[18] Muhammad Aisha; Shanono Ibrahim Haruna. (2019). Transient Analysis and Optimization of a Knuckle Joint. *Kinetik: Game Technology, Information System, Computer Network, Computing, Electronics, and Control*. 4, (2).

[19] Ren, J.W.; Shu, S.R.; Deng, F.F. (2022). *ANSYS Workbench modern mechanical design practical tutorial: finite element analysis - optimization design - reliability design (ANSYS Workbench 现代机械设计实用教程：有限元分析•优化设计•可靠性设计)*, 1st ed.; Chemical Industry Press: Beijing, China, pp. 235-264.

[20] Sharma M P; Mevawala D S; Joshi H; et al. (2014). Static Analysis of Steering Knuckle and Its Shape Optimization. *IOSR Journal of Mechanical and Civil Engineering*, 8, 34-38.

[21] Yu, J.Y. (2022). *Design and Experiment Research of Roller Potato Grading Device (辊式马铃薯分级机设计与试验研究)*. Northeast Agricultural University, Harbin, Heilongjiang, China, June.

[22] Yan, H.D. (2022). Optimization Design of Tension Machine Frame Based on Solidworks and ANSYS Workbench. *Journal of Engineering Research and Reports*. 23, 11-17.

[23] Zhang, X. M.; Zhang, Y. B.; Wang, Y. C. (2020). Improved Design of Three-wheeled Vehicle Headlamp Fixing Bracket Based on UG (基于 UG 的三轮汽车前照灯固定支架改进设计). *Agricultural Equipment & Vehicle Engineering*. 58, 119-124.

[24] Zhang, Y. (2017). *ANSYS Workbench 17.0 Finite Element Analysis from beginner to master (ANSYS Workbench 17.0 有限元分析从入门到精通)*, 2nd ed.; China Machine Press: Beijing, China; pp. 403-425.

[25] Zhao, W. Y.; Yang, J. P.; Dong, X. H.; Huang, B. (2023). Simulation Analysis and Research of Subsoiler Shovel Seat Based on ANSYS Workbench (基于 ANSYS Workbench 的深松机铲座的仿真分析与研究). *China Southern Agricultural Machinery*. 54, 10-14.

[26] Zhou, J.G. (2022). *Study on Key Technologies of Potato Joint Harvest and Primary Classification in Hilly Mountainous Areas (丘陵山区马铃薯联合收获与初选分级关键技术研究)*. Northwest A&F University, Xianyang, Shaanxi, China, May.

[27] Zuo, A. D.; Zhao, Y. Y. (2023). Application of Ansys_Workbench Optimization Module Combined with Limit Load Analysis in Engineering Design (Ansys_Workbench 优化模块结合极限载荷分析在工程设计中的应用). *China Special Equipment Safety*. 39, 19-25.